



HAL
open science

Surface magnetism in the pulsating RV Tauri star R Scuti

Stefan Georgiev, Agnès Lèbre, Eric Josselin, Philippe Mathias, Renada Konstantinova-Antova, Laurence Sabin

► **To cite this version:**

Stefan Georgiev, Agnès Lèbre, Eric Josselin, Philippe Mathias, Renada Konstantinova-Antova, et al.. Surface magnetism in the pulsating RV Tauri star R Scuti. Monthly Notices of the Royal Astronomical Society, 2023, 522 (3), pp.3861-3876. 10.1093/mnras/stad1210 . hal-04098884

HAL Id: hal-04098884

<https://hal.science/hal-04098884>

Submitted on 16 Feb 2024

HAL is a multi-disciplinary open access archive for the deposit and dissemination of scientific research documents, whether they are published or not. The documents may come from teaching and research institutions in France or abroad, or from public or private research centers.

L'archive ouverte pluridisciplinaire **HAL**, est destinée au dépôt et à la diffusion de documents scientifiques de niveau recherche, publiés ou non, émanant des établissements d'enseignement et de recherche français ou étrangers, des laboratoires publics ou privés.

Surface magnetism in the pulsating RV Tauri star R Scuti

Stefan Georgiev ^{1,2}★, Agnès Lèbre,² Eric Josselin,² Philippe Mathias,³ Renada Konstantinova-Antova¹ and Laurence Sabin ⁴

¹*Institute of Astronomy and NAO, Bulgarian Academy of Science, 72, Tsarigradsko Chaussee Boulevard, 1784 Sofia, Bulgaria*

²*LUPM, Université de Montpellier, CNRS, Place Eugène Bataillon, F-34095 Montpellier, France*

³*IRAP, Université de Toulouse, CNRS, UPS, CNES, 57 avenue d'Azereix, F-65000 Tarbes, France*

⁴*Instituto de Astronomia, Universidad Nacional Autónoma de México, Apdo. Postal 877, C.P. 22860 Ensenada, B.C., México*

Accepted 2023 April 14. Received 2023 April 14; in original form 2022 March 31

ABSTRACT

We present the surface magnetic field conditions of the brightest pulsating RV Tauri star, R Sct. Our investigation is based on the longest spectropolarimetric survey ever performed on this variable star. The analysis of high resolution spectra and circular polarization data give sharp information on the dynamics of the atmosphere and the surface magnetism, respectively. Our analysis shows that surface magnetic field can be detected at different phases along a pulsating cycle, and that it may be related to the presence of a radiative shock wave periodically emerging out of the photosphere and propagating throughout the stellar atmosphere.

Key words: stars: AGB and post-AGB – stars: atmospheres – stars: magnetic field.

1 INTRODUCTION

RV Tauri stars are high luminosity pulsating variables. Their light curves show alternating deep and shallow minima in a quasi-periodic manner, the periodicity being sometimes interrupted by irregular intervals due to intrinsic phenomena. During regular parts of the light curve, the photometric variability period P is defined as the time interval between two consecutive deep minima. The values of P are usually between 30 and 150 d (Wallerstein & Cox 1984). Jura (1986) studied the mass-loss rates of RV Tauri stars and concluded that these objects have recently left an evolutionary phase of rapid mass-loss. Considering their luminosities ($\sim 10^3 L_{\odot}$) and formation rate (about 10 per cent of the rate of formation of planetary nebulae) Jura (1986) proposed that they are post-AGB objects in transition from the asymptotic giant branch (AGB) to the White Dwarf stage, which is a very short phase in the lifetime of a star.

R Sct (HD 173819) is the brightest member of the RV Tauri type stars. According to the General Catalogue of Variable Stars (GCVS¹), its visual magnitude ranges between 4.2 down to 8.6 and its photometric variability period is between 138.5 and 146.5 d (with variability from one cycle to another). Because of the strong photometric variability R Sct exhibits, its spectral class also varies significantly: from G0Iae during maximum light to M3Ibe during deep minimum light. From observations taken during the phases of shallow minimum and just after a maximum in the light curve, Kipper & Klochkova (2013) measure the following stellar parameters: $T_{\text{eff}} = 4500$ K, $\log g = 0.0$, and $[\text{Fe}/\text{H}] = -0.5$.

For R Sct, during each pulsation cycle, two accelerations of the atmospheric layers occur, which are caused by the propagation of radiative shock waves (Gillet et al. 1989). By studying the variability

of spectral lines, Lèbre & Gillet (1991a, b) found that the expansion of the stellar atmosphere due to the passing of such shock waves may reach up to a few photospheric radii. Indeed, the propagation of these shocks produces significant ballistic motions in the atmosphere, that can be traced through dedicated spectral features, such as, for example, the splitting of metallic lines and emission in the lines of hydrogen. These studies also show that the two shockwaves associated with one pulsation cycle (a main shock and a secondary shock) appear, respectively, just before the deep and the shallow light minimum, and that they may both be present at the same time, at different altitudes, in the higher part of the extended atmosphere of R Sct. The authors also point out that this complex atmospheric dynamics may be at the origin of the mass-loss the star experiences at this late evolutionary stage.

Since AGB and post-AGB stars are among the main sources of enrichment of the interstellar medium through their winds and mass-loss, the understanding of the origin of these processes is fundamental. An important mechanism, which would be related to mass-loss, involves the presence of magnetic fields. However, their exact role in this process at these late stages of stellar evolution is still poorly understood. For example, while binarity is invoked as a principal shaping agent of the circumstellar envelope (CSE; Decin et al. 2020), magnetic fields could still play an active role in this task (Blackman et al. 2001).

The first discovery of a surface magnetic field in R Sct was reported by Lèbre et al. (2015), who estimate the longitudinal magnetic field $B_l = 0.9 \pm 0.6$ G. Moreover Sabin, Wade & Lèbre (2015) found that the surface magnetic field of R Sct is variable with time, sometimes being not present or below their detection limit of 0.5 G. They also observed a connection between the line profiles resulting from the shock propagation and the Zeeman signatures in circular polarization. On this basis they suggested there could be a link between the dynamical state of the extended stellar atmosphere of R Sct and its surface magnetic field. Such a link has already been proposed for

* E-mail: sgeorgiev@astro.bas.bg

¹<http://www.sai.msu.su/gcvs/gcvs/>

the pulsating variable Mira star χ Cyg (Lèbre et al. 2014), where the shockwave propagation throughout the stellar atmosphere seems to amplify, through compression, a weak surface magnetic field.

The objective of this work is to investigate the magnetism of R Sct during a long-term spectropolarimetric survey, in order to check if there is indeed an interplay between the surface magnetic field and the atmospheric dynamics present in this cool evolved star. The article is organized as follows. Section 2 presents the spectropolarimetric observations used for the study, and the different tools used for their subsequent analysis. The atmospheric dynamics of R Sct is then illustrated in Section 3 from the associated high resolution spectroscopic observations. In Section 4, we present a refined approach to study the surface magnetism in such a pulsating star hosting an extended atmosphere. The circular polarization data (Stokes V profiles) are analysed and the magnetic (Zeeman) origin of the detected signatures is investigated. Section 5 presents briefly the available observations of R Sct in linear polarization, and finally, in Section 6, a summary of the obtained results is given.

2 OBSERVATIONS AND DATA ANALYSIS

2.1 Spectropolarimetric observations

Observations of R Sct were obtained between 2014 July and 2019 August using the Narval instrument (Aurière 2003) on the 2-m class *Télescope Bernard-Lyot (TBL)* at the *Pic du Midi* observatory, France. This high resolution spectropolarimeter has a resolving power $R = 65\,000$ and covers the spectral window between 375 and 1050 nm. The Narval instrument is designed to detect polarization levels (circular or linear) within atomic lines. It allows simultaneous measurement of the full intensity (Stokes I) and the intensity in circular (Stokes V) or linear (Stokes U or Stokes Q) polarization versus wavelength.

Our Narval observations represent the longest monitoring of R Sct ever performed using high resolution spectropolarimetry so far. It corresponds to 6 seasons of observability of R Sct obtained over the course of 6 yr, which will hereafter be referred to as 6 data sets, from set 1 to set 6. All these Narval observations are composed of a number of spectropolarimetric sequences (circular and/or linear polarization), all of which include a high resolution intensity spectrum (Stokes I measurements) and also a high resolution polarization spectrum (in Stokes U , Q or V). With approximately one observation per month (during the seasons R Sct is visible from *Pic du Midi*), linear and circular polarization data have been collected preferably in a single night, or during consecutive nights depending on target observability or weather conditions. Hence, the total data set spans over 67 different dates of observation, 31 of which contain Stokes V measurements, giving access to the information about the surface magnetism. The full log of observations is given in Table 1. The observations that contain measurements on linear polarization are presented in Section 5, but the Stokes Q and U profiles themselves are not examined in details in this study; instead, only their associated high resolution unpolarized spectra (Stokes I) are used to trace the atmospheric conditions of R Sct (in Section 3). Our survey stops at the end of 2019 August, when the TBL was stopped to install the successor of Narval, Neo-Narval. In the interests of keeping an homogeneous data set, we therefore limited the data used in this study to the Narval observations only.

In order to correlate the information on the atmospheric dynamics and the surface magnetism in our data set to the photometric variability of R Sct, the visual light curve of the star was retrieved

from the AAVSO² database, and it is presented in Fig. 1. The dates for which Narval observations were collected are marked on the light curve with red and blue vertical lines for circular and linear polarization, respectively.

During the first part of the monitoring, between 2014 April (HJD = 2456773) and 2016 June (HJD = 2457905), the light curve of R Sct appears regular (showing the usual alternation of deep and shallow minima). However, after this, the next expected deep minimum appears shallow instead, and after that the periodicity is lost. It is restored again in 2019 June (HJD 2458280). The limits of the irregular portion of the light curve between 2016 June and 2019 June are indicated on Fig. 1 with dashed red vertical lines. This irregular portion within the light curve of R Sct then only concerns most of the 4th data set of our monitoring, while the five other data sets are related to regular portions of the light curve (see Fig. 1).

The photometric period of R Sct, when it is apparent (i.e. outside the irregular portion of the light curve in Fig. 1) is variable from one cycle to the next one. We find that the average period length in the first regular part of the observational data set is 141.50 d, while in the second one, after the irregular portion, it is 147.33 d. Using these two period values, and only for Narval observations associated with the regular parts of the light curve (see Fig. 1) we compute the photometric phase according to the following ephemerids:

$$\phi(t) = \frac{t - 2456773.5}{141.5} \quad \text{for sets 1, 2 and 3} \quad (1)$$

$$\phi(t) = \frac{t - 2458280.5}{147.33} \quad \text{for sets 5 and 6.} \quad (2)$$

We use equation (1) for the first regular portion of the light curve (in Fig. 1: between the red star located at HJD = 2456773.5 and the first vertical dashed red line located at HJD = 2457905.5) and equation (2) for the second one (in Fig. 1: after the second vertical dashed red line located at HJD = 2458280.5). We point out that the ephemerids are computed so that the deep minimum for each period corresponds to phase 0 (or to an integer value), which is the convention for RV Tauri stars.

2.2 Data analysis

2.2.1 Least square deconvolution (LSD)

In order to extract the mean polarization signatures from the data, we used the LSD method (Donati et al. 1997) on our Narval data. This method is similar to cross-correlation and uses a numerical line mask to average the profiles of thousands of atomic lines, under the assumption that they have the same shape scaled by a given factor. The result of the LSD procedure is a mean line profile, referenced later as the LSD profile, in heliocentric velocity space, in both full intensity (Stokes I) and polarized light (Stokes $Q/U/V$).

For a given date, when several spectropolarimetric sequences are available (see Table 1), we first performed LSD on the individual sequences, and then combined the obtained results into an averaged LSD output (displayed and analysed through this paper). We note that occasionally for some observations the individual sequences were obtained in two consecutive nights. In these cases, we average together the LSD outputs of the sequences from consecutive nights, i.e. we consider them as a single observation. Such a combining of sequences from consecutive nights is necessary to achieve higher signal-to-noise ratio when using LSD. This is

²<https://www.aavso.org/>

Table 1. Log of spectropolarimetric observations. Calendar and heliocentric Julian dates (HJD) are given in the first two columns. HJD starts from 2450000. The horizontal lines show the limits of the 6 observational sets described in Section 2.1. The phase (calculated according to equations 1 or 2) is given in the third column. The fourth column indicates the number of Stokes $Q/U/V$ sequences collected for each date. The fifth column shows the signal-to-noise ratio (SNR) of the Narval Stokes I spectra. The SNR is computed per spectral pixel at the center of the *echelle* order that contains the maximal signal (this typically corresponds to a wavelength of 731 or 755 nm). When multiple spectra are acquired on a given night, it is the median value of their SNR that is reported in the table. The dates for which the *cool* mask is used in LSD are marked with ‡, and for the other dates, the standard mask is used (see Section 2.2).

Date	HJD	Phase	Sequences	SNR	Date	HJD	Phase	Sequences	SNR
2014/07/15	6854.5	0.57	1Q,1U,2V	994	2016/10/27	7689.3	6.47	1U	868
2014/07/22	6861.4	0.62	10V	765	2016/10/28	7690.3	6.48	2Q	763
2014/09/01‡	6902.3	0.91	1Q,1U	1025	2017/04/18	7862.6	7.70	9V	1179
2014/09/02‡	6903.3	0.92	6V	828	2017/04/20	7864.6	7.71	2U	1333
2014/09/11‡	6912.3	0.98	1Q,6V,1U	855	2017/04/21	7865.6	7.72	2Q	1340
2015/04/13	7126.6	2.50	3V	1021	2017/08/21‡	7987.4	–	6V	1162
2015/04/14	7127.6	2.50	1Q,1U	1067	2017/08/22‡	7988.4	–	2Q	956
2015/04/23	7136.6	2.57	2V	588	2017/09/02	7999.4	–	4Q	753
2015/05/27	7170.5	2.81	3V,1Q,1U	878	2017/09/06	8003.3	–	2Q	1176
2015/06/02	7176.6	2.85	9V	819	2017/09/07	8004.3	–	2U	1650
2015/06/26‡	7200.5	3.02	2U,2Q,9V	1447	2017/09/08	8005.3	–	3V	1451
2015/08/05	7240.4	3.30	2Q,2U	751	2017/10/02‡	8029.3	–	2U	982
2015/08/06	7241.9	3.31	16V	751	2017/10/04‡	8031.3	–	2Q	541
2015/08/10	7245.4	3.34	6V	1010	2017/10/05‡	8032.3	–	3V	1051
2015/08/26‡	7261.4	3.45	2Q	637	2017/10/30‡	8057.3	–	2U	1338
2015/08/28‡	7263.4	3.46	2U,6V	1234	2017/10/31‡	8058.2	–	2Q	1121
2015/10/08	7304.3	3.75	1Q,1U	796	2017/11/01‡	8059.8	–	9V	1134
2015/10/09	7305.3	3.76	6V	796	2018/06/18	8288.5	0.05	2U,2Q	1010
2015/10/29	7325.3	3.90	1Q,1U	950	2018/06/19	8289.5	0.06	3V	761
2015/10/30	7326.3	3.91	5V	1414	2018/07/27	8327.5	0.32	2U,2Q	868
2016/03/17‡	7465.6	4.89	1U,1Q	883	2018/07/28	8328.5	0.33	3V	1142
2016/05/04	7513.6	5.23	1U,1Q	1262	2018/08/15	8346.5	0.45	2Q,2U	1166
2016/05/15	7524.6	5.31	3V	1044	2018/08/31	8362.4	0.56	2Q,2U	938
2016/05/20	7529.6	5.34	3V	1105	2018/09/08	8370.4	0.61	3V	1227
2016/06/02	7542.6	5.44	1U,1Q	1083	2018/10/24‡	8416.3	0.92	2Q	840
2016/06/22	7562.5	5.58	1U,1Q	1141	2018/10/25‡	8417.3	0.93	2U	954
2016/07/12	7582.5	5.72	1U,1Q	1436	2019/06/15	8650.5	2.51	3V,2Q	1090
2016/07/24	7594.4	5.80	3V	1147	2019/06/27	8662.5	2.59	3V	1153
2016/08/03	7604.4	5.87	1U,1Q	1049	2019/07/15	8680.4	2.71	2Q,2U	1338
2016/09/01	7633.3	6.08	1Q,1U	759	2019/07/18	8683.5	2.74	3V	1274
2016/09/24	7656.4	6.24	1Q	717	2019/08/05	8701.5	2.86	2U	1088
2016/09/28	7660.3	6.27	3V,1U	873	2019/08/13	8709.4	2.91	2Q	847
2016/10/03	7665.3	6.30	3V	1103	2019/08/31‡	8727.4	3.03	6V	755

possible in the case of R Sct because there is no noticeable variability on such short time-scales (1 d) between the individual sequences (neither in the intensity spectra, nor in the polarized profiles).

To study the surface magnetic field in R Sct, we applied the LSD method on the observational data to extract the mean Stokes I and Stokes $U/Q/V$ profiles of atomic spectral lines. In order to do this, we first built a line mask computed from a MARCS model atmosphere (Gustafsson et al. 2008) with parameters compatible with the known parameters of the star ($T_{\text{eff}} = 4500$ K, $\log g = 0$, microturbulence velocity $\xi = 2$ km s $^{-1}$ and $[\text{Fe}/\text{H}] = -0.5$), and using atomic linelists extracted from the Vienna Atomic Line Database (VALD; Kupka et al. 1999). We kept the atomic lines of all chemical elements except those elements that have lines known to exhibit emission and/or trace the very high atmosphere (H, He, Ca) and lines known to be affected by interstellar contamination (e.g. Na and K). Only lines with a central depth greater than 0.2 of the level of the continuum were considered in the mask computation. An example of an LSD output (computed with such a numerical mask gathering about 17 000 atomic lines) is shown in Fig. 2.

An LSD profile is normalized by three independent coefficients. These are the equivalent wavelength, equivalent depth, and equivalent Landé factor (λ_{eff} , d_{eff} , and g_{eff} , respectively). These three coefficients do not, in general, correspond to the respective mean values of the wavelength, depth, and Landé factor of the atomic lines used in the LSD procedure. In order to avoid differences in this normalization when comparing LSD profiles of different observations (as it is done in this work), in Donati et al. (1997) two parameters are introduced that are functions of λ_{eff} , d_{eff} , and g_{eff} : a mean intensity weight W_{int} and a mean polarization weight W_{pol} . When both of these weights are equal to 1, the resulting LSD profile does not depend on λ_{eff} , d_{eff} , and g_{eff} . In this paper, all LSD calculations are performed in this way, with $W_{\text{int}} = W_{\text{pol}} = 1$, which allows the comparison of LSD profiles obtained on different nights of observation.

2.2.2 Atomic line masks

In the course of its photometric variability, R Sct changes significantly not only its visual magnitude, but also its spectral type, hence its effective temperature T_{eff} . From the literature, it is known that during a shallow minimum light and around a maximum luminosity,

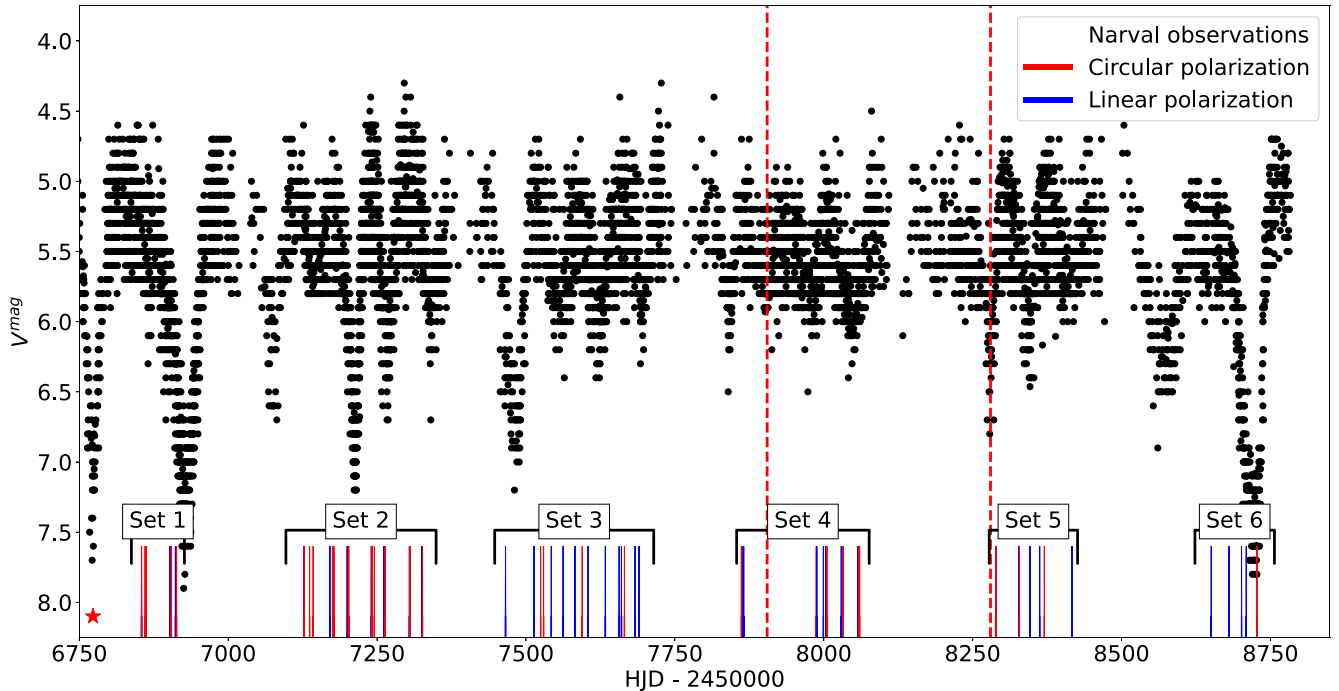


Figure 1. Visual light curve of R Sct from AAVSO. The collected spectropolarimetric observations (see Table 1) are indicated by vertical lines (red and blue lines for the circular and linear polarization observations, respectively) and the six observational sets are noted. The limits of the irregular interval of photometric variability (see Section 2.1) are represented by the two dashed red vertical lines. The red star indicates the date selected to be the reference point (i.e. the beginning of period 0) in the first phase computation (see equation 1); the reference point in the second phase computation (see equation 2) corresponds to the rightmost vertical dashed red line, i.e. the date the regularity of the light curve is restored.

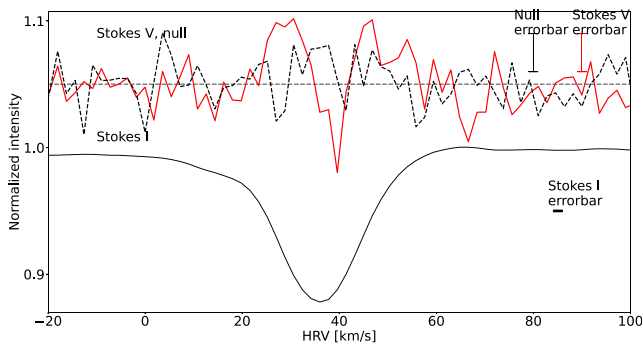


Figure 2. Example of the LSD profiles (Stokes I , solid black curve, and Stokes V , solid red curve) for R Sct at the date of 2014/09/02, corresponding to a definite detection (see Section 2.2.3). The dashed black curve displays the null diagnostic that has to stay featureless to confirm the absence of instrumental effect. The null and Stokes V profiles are shifted vertically and magnified for display purposes, and their zero level is indicated with a dashed horizontal line. The mean errorbars of the Stokes I , null and Stokes V profiles are also shown and labelled.

the effective temperature of the star is 4500 K (Kipper & Klochkova 2013). However the spectral type changes to a much later one near a deep minimum light, suggesting different atmospheric conditions through a lower effective temperature. Our Narval observations also show that TiO molecular bands appear in the high resolution spectra of R Sct collected close to a deep minimum light, indicating a significant decrease in T_{eff} . This means that using a single LSD mask computed with a unique effective temperature reference to treat our whole data set may not be relevant. A more reliable

result would be obtained if, instead, the observations obtained around a deep minimum light (hence showing these TiO band features) are treated using a LSD mask computed for a lower effective temperature closer to that of the star at this photometric stage.

To estimate the effective temperature of R Sct around a deep minimum light, we used the code *Turbospectrum* (Alvarez & Plez 1998; Plez 2012) to construct a series of synthetic spectra around two molecular bands of TiO (TiO 7054 and TiO 7589 Å) which are detected in the spectra of R Sct during these specific phases. To construct the synthetic spectra, we used again linelists extracted from the VALD data base and MARCS model atmospheres computed for $1 M_{\odot}$, $\log g = 0.0$, $\xi = 2 \text{ km s}^{-1}$ and $T_{\text{eff}} = 4500, 3800, 3600,$ and 3400 K . We used the built-in procedure in *Turbospectrum* to take into account the instrumental profile of Narval and to introduce the effects of rotational and macroturbulent velocities. Regarding the latter two velocities, neither value is known for R Sct, and we assigned to $v \sin i$ and to v_{mac} the ad hoc value of 5 km s^{-1} , which is a reasonable value for AGB and post-AGB stars (Georgiev et al. 2020). It must be noted that there is no particular reason to pick these exact values, and that they have no impact on the task at hand. The objective is indeed not to determine accurate stellar parameters, but instead only to give a rough estimation of T_{eff} ; for this purpose, any reasonable pair of these two velocities would suffice.

In Fig. 3, we compared the computed synthetic spectra to two observational spectra of R Sct, obtained on 2015/04/23 (corresponding to a shallow minimum light) and on 2019/08/31 (collected at the exact time of a deep minimum light). It can be seen from the synthetic spectra that the 7054 Å TiO band (Fig. 3a) begins to develop only at temperatures below 3800 K. On the other hand, this band is present in the observation collected around a deep minimum light (solid black

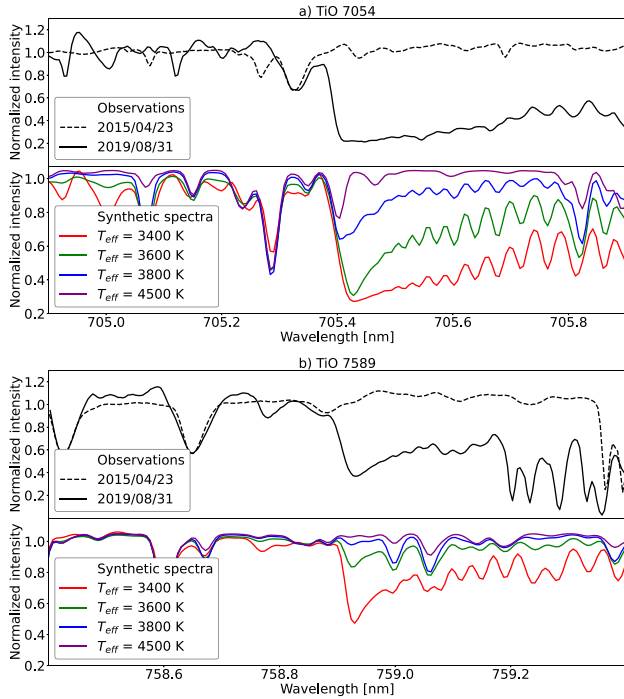


Figure 3. TiO 7054 Å (panel ‘a’) and TiO 7589 Å (panel ‘b’) bands in the spectra of R Sct. For each TiO band, the top subpanel shows two observed spectra, obtained on 2015/04/23 (corresponding to a shallow minimum) and 2019/08/31 (corresponding to a deep minimum). The bottom subpanels show synthetic spectra computed for four different values of T_{eff} .

line), but not in the one collected around a shallow minimum light (dashed black line). This is consistent with the 4500 K estimation Kipper & Klochkova (2013) obtain for the shallow minimum and maximum phases. The synthetic spectra also show that this TiO band continues to develop in both depth and width as temperature decreases until $T_{\text{eff}} = 3400$ K. Further decreasing the temperature makes the band more shallow instead. As displayed in Fig. 3b, the 7589 Å TiO band) is again only present in observations obtained around a deep minimum light (solid black line). In the synthetic spectra, this band is not present at 4500 K and not even at 3800 K. It begins to develop only at 3600 K and grows in depth and width as temperature decreases, reaching noticeable depth in the 3400 K spectrum. We can draw two firm conclusions from this: (1) around a shallow minimum light, the effective temperature of R Sct is above 3800 K, in good agreement with the measurements of Kipper & Klochkova (2013); (2) around a deep minimum light, the effective temperature is below 3800 K, since both TiO bands appearing in the spectra are best described by the synthetic spectra computed for 3400 and 3600 K (see Fig. 3), which well matches the M spectral type expected during times of deep minimum.

For this reason, we decided to perform LSD in the following manner:

- for all observations in which TiO bands are absent, i.e. all except those obtained around a deep minimum light – using a mask computed for $T_{\text{eff}} = 4500$ K (henceforth, the *standard* mask);
- for the only observations in which TiO bands are present, i.e. those obtained around a deep minimum light – using a mask computed for $T_{\text{eff}} = 3500$ K (henceforth, the *cool* mask).

A last justification for the use of such a *cool* mask (at deep minimum phases) is that even if it does not perfectly reflect the effective temperature of R Sct during a deep minimum light, it

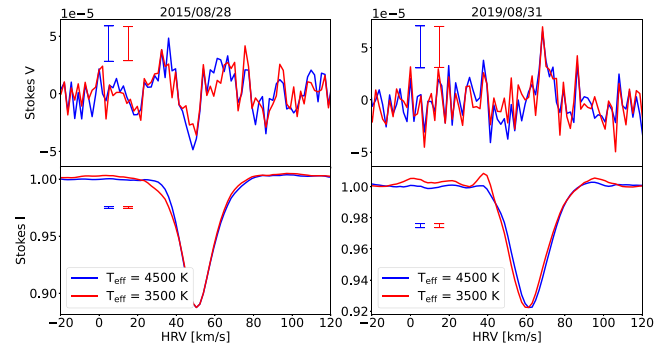


Figure 4. Comparison between the LSD profiles obtained with the *standard* (blue) and *cool* (red) masks for two observations obtained around a deep minimum light – 2015/08/28 (left) and 2019/08/31 (right). The upper panels show the respective Stokes V profiles, while the bottom panels show the intensity profiles for both observations. The mean errorbars of the Stokes I and Stokes V profiles are indicated for both masks.

certainly gives a better approximation than the *standard* mask does. The other stellar parameters, the *standard* and *cool* masks were computed for, are $\log g = 0.0$, microturbulence of 2 km s^{-1} and $[\text{Fe}/\text{H}] = -0.5$, in agreement with Kipper & Klochkova (2013). The total number of lines in each of the two masks is approximately 17 000, with the *standard* mask containing slightly more strong lines (with a central depth larger than the average) than the *cool* one.

In Fig. 4, a comparison between the LSD profiles obtained with the *standard* (in blue) and *cool* (in red) masks is presented for two observations obtained around a deep minimum light (2015/08/28 and 2019/08/31). It can be seen that differences are present in the shape and amplitude of both the Stokes V (upper panels) and the intensity profiles (bottom panels), which justifies the use of the *cool* mask for observations where TiO bands are present in the spectrum.

As we shall see in Section 4, the selection of lines in these LSD masks can be constrained even further in order to trace only the contribution of the photosphere (in this work for convenience by ‘photosphere’ we mean the bottom part of the atmosphere). But first, in the following section, we infer the atmospheric dynamics of R Sct along our Narval monitoring (covering about 2000 d), by studying spectral indicators.

2.2.3 Detection of polarized signatures

In order to evaluate the presence or lack of signature in the polarized LSD profile, we used the *specpolFlow* package³ for treatment of spectropolarimetric observations. This package provides a routine for the calculation of the probability that the observed polarized signal is consistent with the null hypothesis of no magnetic field, or the false alarm probability (FAP), evaluated from χ^2 . We then take the calculated value of the FAP and apply to it the criteria defined by Donati et al. (1997) in order to classify an observation as a no detection (ND, $\text{FAP} > 10^{-2}$), a marginal detection (MD, $10^{-2} > \text{FAP} > 10^{-4}$), or a definite detection (DD, $\text{FAP} < 10^{-4}$). This detection parameter is provided in column 4 of Table 2.

3 ATMOSPHERIC DYNAMICS

The first qualitative model of the pulsation of the photosphere of R Sct was introduced by Gillet et al. (1990). From spectroscopic

³<https://github.com/folsomcp/specpolFlow>

Table 2. Log of Stokes V observations and associated B_l values. Calendar and HJD are given in the first two columns. HJD starts from 2450 000. The third column lists the phase calculated from equations (1) and (2). The fourth column indicates the type of detection: DD, MD, or ND (see Section 2.2.3). The last two columns present the B_l value and its errorbar, both computed from the $\chi_{\text{high}}^{\text{cool}}$ LSD profiles. The dates for which the $\chi_{\text{high}}^{\text{cool}}$ mask is used are indicated with the symbol †, and for the rest, the $\chi_{\text{high}}^{\text{standard}}$ mask is used (see Section 2.2).

Date	HJD	Phase	Detection ($\chi \geq 2$ eV)	B_l [G] ($\chi \geq 2$ eV)	σ [G] ($\chi \geq 2$ eV)
2014/07/15	6854.5	0.57	MD	−1.41	1.28
2014/07/22	6861.4	0.62	DD	−0.56	0.36
2014/09/02†	6903.3	0.92	DD	−0.48	0.56
2014/09/11†	6912.3	0.98	DD	−1.84	0.71
2015/04/13	7126.6	2.50	ND	−0.18	0.52
2015/04/23	7136.6	2.57	DD	1.18	0.65
2015/05/27	7170.5	2.81	ND	−0.20	0.50
2015/06/02	7176.6	2.85	DD	0.20	0.29
2015/06/26†	7200.5	3.02	ND	−0.08	0.37
2015/08/06	7241.9	3.31	MD	−0.57	0.46
2015/08/10	7245.4	3.34	MD	1.01	0.60
2015/08/28†	7263.4	3.46	MD	−1.55	0.84
2015/10/09	7305.3	3.76	ND	0.11	0.35
2015/10/30	7326.3	3.91	ND	0.61	0.49
2016/05/15	7524.6	5.31	ND	0.39	0.43
2016/05/20	7529.6	5.34	DD	0.55	0.53
2016/07/24	7594.4	5.80	ND	0.45	0.29
2016/09/28	7660.3	6.27	ND	0.32	0.69
2016/10/03	7665.3	6.30	ND	0.90	0.76
2017/04/18	7862.6	7.70	MD	0.45	0.52
2017/08/21†	7987.4	–	ND	−0.53	0.58
2017/09/08	8005.3	–	ND	0.70	1.30
2017/10/05†	8032.3	–	ND	0.11	1.24
2017/11/01†	8059.8	–	MD	3.21	1.31
2018/06/19	8289.5	0.06	MD	−2.91	1.46
2018/07/28	8328.5	0.33	ND	0.89	0.59
2018/09/08	8370.4	0.61	ND	0.37	0.91
2019/06/15	8650.5	2.51	ND	0.76	0.78
2019/06/27	8662.5	2.59	ND	−0.22	0.76
2019/07/18	8683.5	2.74	DD	−1.58	0.35
2019/08/31†	8727.4	3.03	ND	−2.83	1.28

observations, these authors reported that two shockwaves propagate throughout the stellar atmosphere along one pulsation cycle. The first (main) shockwave is found to emerge from the photosphere just before the phase of deep photometric minimum (set at $\phi = 0$). This main shock is strong and it is supposed to produce a large elevation of the atmosphere, followed by a subsequent infalling motion due to the force of gravity (ballistic motion). A secondary (and weaker) shockwave emerges from the photosphere just before the occurrence of a shallow photometric minimum around $\phi = 0.5$, while the main shock is vanishing in the upper atmosphere.

This work was extended by Lèbre & Gillet (1991a, b) who investigated the profile variations of selected spectral lines which turned out to be good indicators of the motions at the photospheric level, and of ballistic motions taking place in the upper atmosphere.

3.1 Variability of the H α line

In our Narval spectra of R Sct, the H α line shows an emission component which varies in strength along the photometric phase. The left-hand panel of Fig. 5 shows the profile variation of the H α line along the observational data sets 2 and 3. We selected these two

sets because they offer the best phase coverage with, respectively, 15 and 16 different observational dates (representing ~ 50 per cent of the total number of observations in our survey of R Sct). Hence, the time variations of dedicated line profiles over several pulsation cycles covering a large portion of the regular part of the light curve (see Fig. 1 and Table 1) can be investigated. In our study, we use the value of the stellar rest-frame velocity $v_{\text{rad}} = 42.47 \text{ km s}^{-1}$, recently derived by Kunder et al. (2017). We shall use this value only as a reference point to label the components of spectral line profiles either ‘blueshifted’ or ‘redshifted’ with respect to it.

It can be seen in Fig. 5 that H α shows an emission component with variable amplitude, which is blueshifted with respect to the rest-frame velocity (v_{rad}) of R Sct. H α also shows a variable profile which consists of an absorption component, usually redshifted with respect to v_{rad} . It can be also seen that the emergence of the main shockwave from the photosphere (expected around the phase $\phi = 0$) usually results into a strong H α emission component (e.g. on 2015/10/29, before the minimum light occurring on 2015/11/13 and on 2016/03/17, before the minimum light occurring on 2016/04/02). This is in agreement with the work of Gillet et al. (1989), who presented the complex H α profile as a full emission originating from the front of a radiative shock wave, i.e. from a narrow region where the temperature and pressure conditions are favourable to produce such an intense emission line; then the cool hydrogen (either static or relaxing) located above the shock front, introduces an absorption component to the central and/or redshifted part of the line. The secondary shock, while weaker than the main one, is also detectable through an H α emission around the phase $\phi = 0.5$ (i.e. around a shallow photometric minimum). This emission feature then decreases until a new intense emission occurs due to the emergence of a new main and strong shock. A few dates also show a very faint H α emission (e.g. 2015/06/26 at $\phi = 3.02$) or even no emission at all (e.g. 2016/10/27 at $\phi = 6.47$) illustrating the few moments when the atmosphere is almost homogeneously relaxing in a global infalling motion.

3.2 Variability of metallic lines

To study the motions of the atmospheric layers of R Sct during the longest high resolution spectropolarimetric monitoring ever realized for a post-AGB star, we explore the profile variations of metallic lines. Schwarzschild (1952) proposed a mechanism to explain the variations of atomic spectral lines detected in variable pulsating stars hosting shock waves propagating throughout their atmosphere. Indeed the passing of a shock wave through the stellar atmosphere first makes the layers closest to the photosphere move upwards (towards the observer), thus causing the spectral lines formed in these layers to be blueshifted; after the shock has passed, these same layers, as they are relaxing, fall ballistically downwards (away from the observer), thus causing the spectral lines to be redshifted. This Schwarzschild’s mechanism also predicts the possibility for some metallic lines to appear through a double profile, when the shock is strong enough to decouple two velocity regions along the same line of sight. In that case, the bottom part of a large layer of line formation is moving upwards (as lifted up by the passage of a shock wave) while its upper part, located above this shock front, is still relaxing. This basic scenario may be even more complicated in the case of a very extended atmosphere, where the imprints -on atomic metallic lines- of two consecutive shockwaves may be present at the same time, as it has been shown to be the case for R Sct by Lèbre & Gillet (1991b).

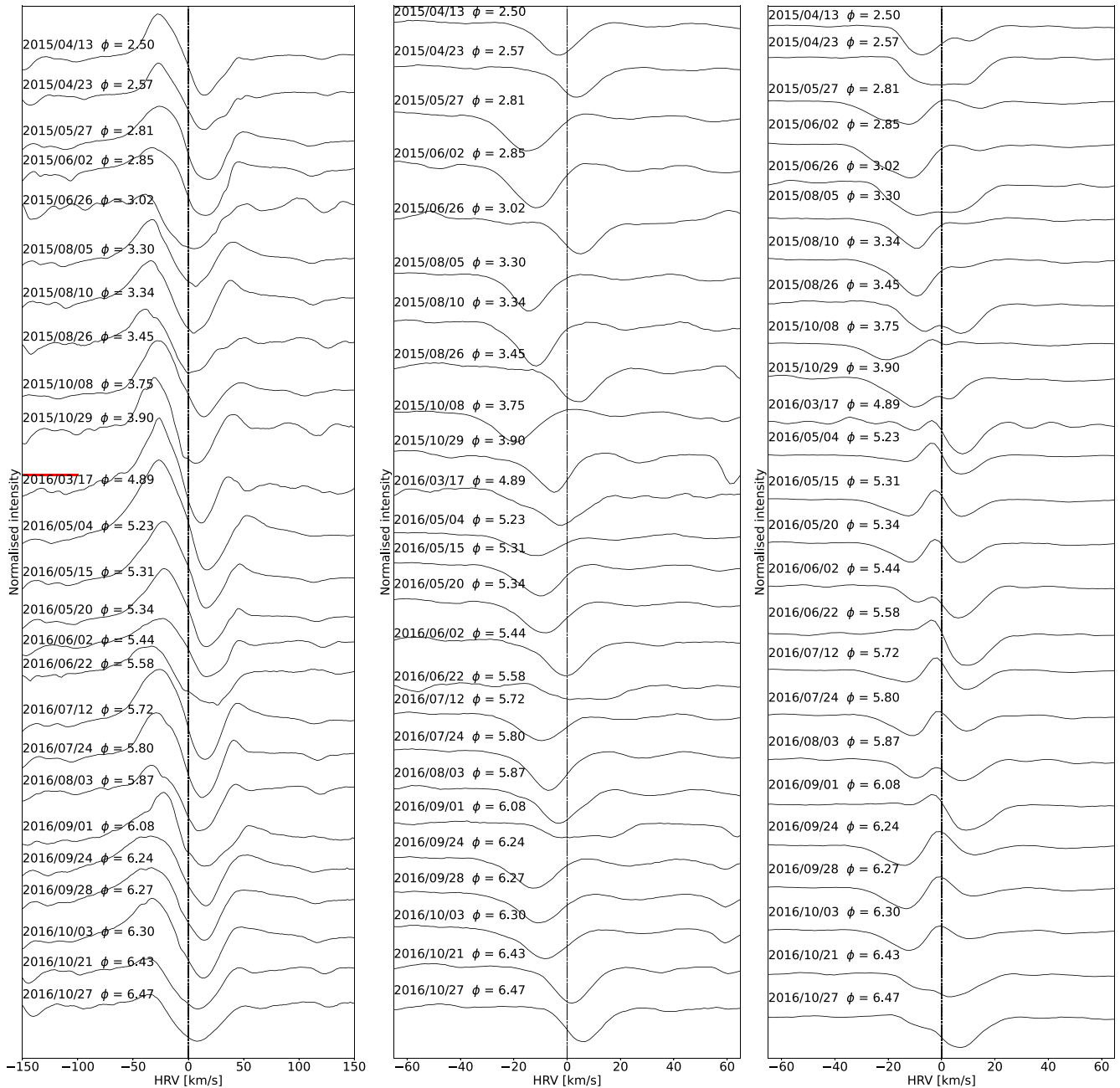


Figure 5. Time variation of the $H\alpha$ line (left-hand panel), FeI 6569 Å; (middle), and TiII 5866 Å; (right) profiles in the spectra of R Sct during data sets 2 and 3. The red horizontal line indicates the boundary between set 2 and set 3. Each observation is shifted vertically for display purposes, and its date is indicated on the top left side, with its phase (computed from equation 1). The rest-frame velocity of R Sct is indicated with a vertical dashed line. When observations from consecutive dates are available, only one date is presented, since no visible difference in the line profile can be appreciated on such a very short time-scale.

In the spectra of R Sct, atomic lines of elements such as Fe and Ti display profiles that vary with the photometric phase, being either fully blueshifted, double-peaked or fully redshifted. According to Lèbre & Gillet (1991a, b), profile variations of FeI line (λ 6569 Å) and TiI line (λ 5866 Å) are good diagnostics to investigate the pulsation motions of their formation regions: the photospheric region, and the upper atmosphere, respectively. Those lines appear to be free from atomic or molecular blend, even at the coolest phases along the pulsation cycle.

3.2.1 The lower atmosphere of R Sct

The profile variation of the FeI 6569 Å line during observational sets 2 and 3 (between April 2015 and October 2016, see Table 1) is shown in the middle panel of Fig. 5. It can be seen from this figure that this line mostly shows a single Gaussian profile (with the exception of very few dates such as 2016/06/22 and 2016/09/01), either blueshifted or redshifted with respect to the restframe velocity of R Sct. Following the Schwarzschild mechanism (Schwarzschild 1952), this corresponds respectively to phases at which the layer of

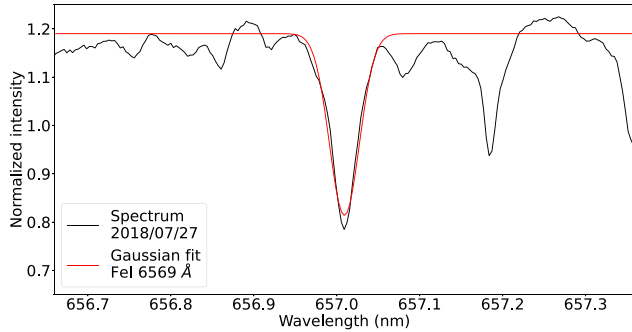


Figure 6. An example of a Gaussian fit (in red) to the Fe I 6569 Å line in the spectrum of R Sct obtained on 2018/07/27 (in black).

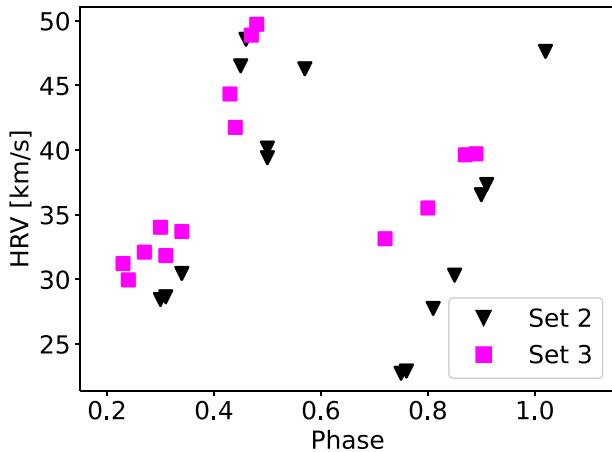


Figure 7. Radial velocity curve of the near-photospheric layers of the atmosphere of R Sct obtained from Gaussian fits on the Fe I 6569 Å line. Points obtained from set 2 and from set 3 are displayed with different coloured symbols.

formation of this atomic line is rising (for the blueshifted profiles) or falling (for the redshifted ones). The absence of a clear double-peak profile of the Fe I 6569 Å line in most of the observations shows that the layer in which this line forms is very narrow and thus is affected only by a single global motion (upward or downward) at any given time. Lèbre & Gillet (1991a) showed that the Fe I 6569 Å line is formed in a narrow region close to the photosphere, this line can thus be used to trace the motion of the photosphere, and hence the periodic emergence of shockwaves.

In order to trace the emergence of shockwaves through the photosphere of R Sct, the radial velocity curve of the Fe I 6569 Å line was constructed by fitting its profile with a Gaussian function in the spectra of R Sct obtained during observational sets 2 and 3. An example fit is shown in Fig. 6 for the observation taken on 2018/07/27. The radial velocity curve is shown in Fig. 7. In this figure, a regular global motion (up and down) of the explored photospheric region is clearly seen. It can be noticed that there are indeed two upward accelerations per photometric period, found around phases $\phi = 0$ and $\phi = 0.5$, which correspond, respectively, to the times of deep and shallow photometric minima, confirming the results of Gillet et al. (1989). The observed dispersion in the radial velocity curve most likely corresponds to cycle-to-cycle variations, as the intensity of the shocks is probably different for one cycle to the other.

3.2.2 The upper atmosphere of R Sct

Lèbre & Gillet (1991a) showed that the Ti I 5866 Å line is formed in the upper atmosphere of R Sct, as this line appears more perturbed by ballistic motions along a pulsation cycle. The time variability of the profile of this spectral line during sets 2 and 3 is shown in the right-hand panel of Fig. 5. We see that the behaviour of this line profile is indeed very different from that of the Fe I 6569 Å line: complex and strongly variable profiles, both single and double-peaked, are observed on different dates. Following the Schwarzschild mechanism, since for some phases we can report double-peaked profiles (e.g. on 2015/08/26, 2016/05/15, and 2017/10/05), this suggests that the Ti I 5866 Å line is formed in a large geometric layer of the upper atmosphere that can be affected – at a given date – by more than one dynamics (i.e. upward and downward motions within the considered thick layer). At the dates double line profiles are reported, at least two different dynamics are thus present within this extended atmospheric layer, resulting from the outward propagation of a shockwave. On the contrary very few dates (e.g. on 2015/08/05, 2016/03/17) present the Ti I 5866 Å line through a single Gaussian profile (blueshifted and redshifted, respectively) suggesting the atmospheric layer is affected by a global motion.

3.3 Atmospheric dynamics: summary

The analysis of the variability of the H α and Fe I 6569 Å line profiles (however limited to data from set 2 and set 3) confirms the results of Gillet et al. (1989), who found that two shockwaves per photometric period emerge from the photosphere of R Sct around the deep and shallow photometric light minima (or, equivalently, just before phases $\phi = 0$ and $\phi = 0.5$). Considering also the Ti I 5866 Å line variability, it is obvious that spectral lines originating from layers of different altitudes and different thickness are also affected by the propagating shockwaves in different ways: ‘photospheric’ lines (i.e. lines which form in a very narrow region near the photosphere, such as the Fe I 6569 Å line) always point to a single global motion – upward or downward – when affected by the passing of a new shockwave, and also indicate the moment at which such a shock emerges from the photosphere; lines that form in wider regions of the atmosphere (such as the Ti I 5866 Å line), on the other hand, may trace more than one dynamics, depending on the location of the shockwave.

4 THE SURFACE MAGNETIC FIELD

4.1 A refined approach

The LSD Stokes V profiles computation described in Section 2.2 is undertaken along the ‘classical’ way when studying surface magnetic fields using high resolution spectropolarimetry. However, before going any further in our analysis, we must consider that this usual approach may not be the best one to use in the case of stars hosting strong pulsations and shockwaves propagating in their atmospheres, such as R Sct. These stars have indeed very extended atmospheres and, at a given time, different atmospheric layers might be affected by very different dynamics. This is precisely what has been illustrated through the investigation of the Fe I 6569 Å and Ti I 5866 Å lines in Section 2.2.2. Thus, an LSD line mask computed without considering the conditions under which spectral lines form (like the *standard* and *cool* masks involved in Section 2.2.2) will surely mix together information from very different altitudes with various physical conditions, surely affected, at any given moment in

time, by different dynamics. This means that the use of line masks described in Section 2.2.2 would yield LSD profiles combining the full complexity of the atmospheric motions, which may however be different for the photospheric region and for the upper atmosphere. Because our objective is to study the *surface* magnetic field (i.e. its condition at the level of the photosphere), introducing information from the higher atmosphere is certainly not the best approach. Hence, new LSD masks have to be constructed based on a refined method for lines selection.

4.2 Lines selection by excitation potential

The higher the excitation potential (χ) of atomic lines is, the less extended their zone of formation in the stellar atmosphere is. In particular, lines with large χ can only be formed in a thin layer near the photosphere. This narrow region is expected to be affected, at any given moment in time, by only one dynamical effect: an upward global motion due to the presence of a shock wave passing through it, or a downward global motion due to the relaxation of this layer after the passage of such a shock. For example, the Fe I 6569 Å line, which was shown in Section 3.2.1 to be formed only in a narrow region near the photosphere of R Sct, has an excitation potential of 4.7 eV (according to the VALD data). On the other hand, lines which have a low excitation potential can be formed under a wider variety of conditions, met both at the photospheric layers and also at higher altitudes. These lines are thus expected to combine the complexity of a large portion of the stellar atmosphere, which may contain layers affected by different dynamics – upward and downward motions. For example, the Ti I 5866 Å, shown in Section 3.2.2 to be formed in an extended region of the atmosphere of R Sct, has an excitation potential of 1.06 eV (according to the VALD data).

This effect is observed for all lines with similar excitation potentials, but in the case of cool stars, it can be illustrated for only a handful of metallic lines, which are not affected by molecular veiling, or through a cross-correlation profile, as done by Alvarez et al. (2000) for Mira stars and by Josselin & Plez (2007) for red supergiant stars.

This physical scenario is presented schematically in Fig. 8. In the upper panel of this figure, a schematic representation of the atmosphere of R Sct is shown (not up to scale). Periodically, a shockwave emerges from the photosphere. The narrow region just above the photosphere is affected by the shock and moves in a global upward motion. The higher atmosphere, however, is not yet affected by this shock; instead, it is moving down, falling ballistically after having been lifted in the past by a previous shockwave. An LSD mask χ_{high} which contains only lines with excitation potential high enough to probe only the atmospheric layers lying close to the photosphere would hence yield an LSD profile showing a fully blueshifted intensity profile, since all these layers are globally moving away from the star. If there is a surface magnetic field above the detection threshold, the LSD profile would also show a Stokes V signature associated with the blueshifted intensity profile (see bottom panel in Fig. 8).

On the other hand, an LSD mask χ_{low} containing lines with lower excitation potential which may be formed at any altitude in the atmosphere of the star would probe both the photosphere and the higher atmosphere: it would yield an LSD profile containing a mixture of information from both the layers adjacent to the photosphere (which are moving globally upwards) and the higher layers of the atmosphere (which are moving globally downwards as they are relaxing after the passage of a previous shock). This means that the intensity profile will present a double peak according to

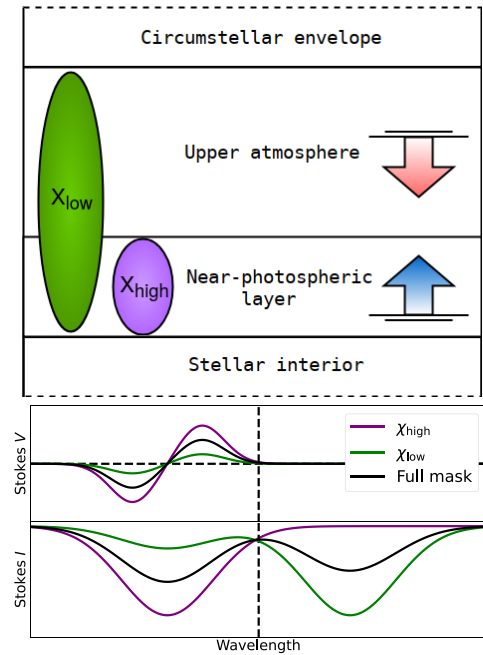


Figure 8. Upper panel: a schematic representation (not up to scale) of two global motions in the atmosphere of R Sct – an upward one in the near-photospheric layers, caused by the passing of a radiative shockwave, and a downward one in the higher atmosphere, caused by the gravitational infall occurring after the propagation of a previous shockwave. Bottom panel: a sketch of the LSD profiles that are expected to be obtained using a mask that is restricted to lines with high χ which probe only the near-photospheric layers of the atmosphere (purple), low χ which probe the same layers plus the higher atmosphere (green), and a mask which contains a mixture of both (black).

the Schwarzschild mechanism. On the contrary, as the intensity of the magnetic field decreases with altitude, a magnetic field above the detection threshold will be only observed in deep/photospheric layers, and thus associated with the blueshifted component of the Stokes I profile. Using a mask containing lines predominantly formed in the higher layers will dilute the signal and thus lead to Stokes V signature with a lower amplitude than the one obtained using the χ_{high} mask. Finally, an LSD line mask which contains all atomic lines regardless of their excitation potential (i.e. containing all the lines in both the χ_{high} and χ_{low} masks) would produce an LSD profile similar to the one shown in black in the bottom panel of Fig. 8: containing information predominantly from the near-photospheric layer, since both the high- and low excitation potential lines trace the conditions in it, but also information from the higher atmosphere, which is not relevant when studying magnetism and dynamics at the photospheric level. A detailed study on the dependency of the depth of line formation on excitation potential is presented in Josselin & Plez (2007) (more specifically their Section 3.1).

To examine the impact lines with different excitation potential have on the LSD profiles, we performed a test by splitting the *standard* LSD mask into two sub-masks: one with $\chi < 2$ eV (7903 lines) and one with $\chi \geq 2$ eV (9031 lines). These masks will hereafter be referred to, respectively, as $\chi_{\text{low}}^{\text{standard}}$ and $\chi_{\text{high}}^{\text{standard}}$. We picked 2 eV to be the separation limit because this value had to be high enough to successfully restrict the LSD process to the near-photospheric layers of the atmosphere and at the same time low enough to allow for a sufficient number of lines in the mask, in order to get Stokes V signatures with high SNR. We then applied the LSD method using

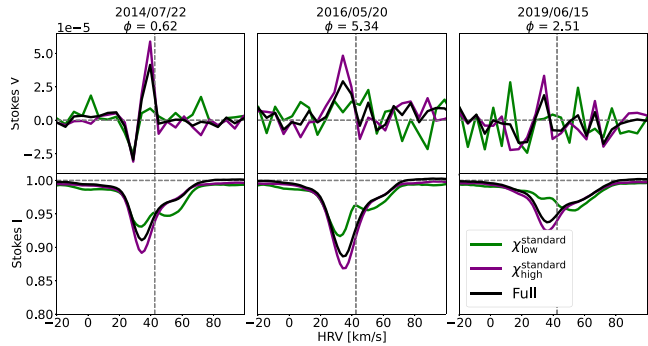


Figure 9. Comparison between the LSD profiles obtained with the $\chi_{\text{low}}^{\text{standard}}$ (containing 7903 lines, in green), $\chi_{\text{high}}^{\text{standard}}$ (containing 9031 lines, in purple), and full *standard* (containing 16 934 lines, in black) line masks for 2014/07/22 (left column), 2016/05/20 (middle column), and 2019/06/15 (right column). The Stokes V and intensity profiles are shown in the top and bottom rows, respectively. The zero-level of the Stokes V and the continuum level of the intensity are indicated by the dashed horizontal lines in their corresponding panels, and the radial velocity of R Sct is indicated by the dashed vertical line.

both sub-masks to the observations obtained outside a deep minimum light and compared the results. We did the same for observations collected around deep minimum light but treated with the *cool* mask instead. An example of this comparison is shown in Fig. 9. In this figure, it can be seen that the Stokes I profiles obtained with the $\chi_{\text{low}}^{\text{standard}}$ and $\chi_{\text{high}}^{\text{standard}}$ sub-masks have completely different shapes, showing that indeed the lines used for their construction probe layers of the atmosphere with different extent, and which are also affected by different dynamics, and thus should be mixed together only with great caution. It can also be seen in Fig. 9 that the lines with higher excitation potential, which are expected to trace – at a given moment in time – only one atmospheric dynamics at the photospheric level, show a stronger degree of circular polarization. Their associated V -signal is also blueshifted, and it appears to be linked to the blue-component of the I -profile. While for some observations the $\chi_{\text{high}}^{\text{standard}}$ sub-mask yields LSD profiles with clear Stokes V signatures, the $\chi_{\text{low}}^{\text{standard}}$ sub-mask never produces any LSD profiles with a signature in Stokes V . From this figure, one can appreciate the level of contamination low excitation potential lines introduce to the signal originating from the photosphere.

The Stokes I and Stokes V profiles obtained using the $\chi_{\text{high}}^{\text{standard}}$ sub-mask are similar in shape to the ones obtained using the full *standard* mask. This is in agreement with the scenario presented in Fig. 8, since it shows that while both lines with low and high excitation potentials (which together constitute the full *standard* LSD mask) trace the photospheric layer, only the higher excitation potential ones are limited strictly to it, while lines with lower χ also contain information from higher atmospheric layers (and hence unrelated to the surface magnetic field). It must be noted that the LSD profiles we obtain using the χ_{low} submasks (both *standard* and *cool*) show no trace of Stokes V signatures in any observation. This means that the extended atmosphere of R Sct (probed by low excitation potential lines) as a whole does not show traces of a magnetic field, but only its bottom layers (probed by high excitation potential lines) do, which is a further justification of the restriction $\chi \geq 2$ eV we use in our LSD analysis.

From what is seen in Fig. 9, it can also be concluded that while the photospheric layers of R Sct show traces of a variable magnetic field, the atmosphere of the star as a whole (represented by the $\chi_{\text{low}}^{\text{standard}}$ sub-mask) does not. Furthermore, for the observations where the $\chi_{\text{high}}^{\text{standard}}$

one shows clear Stokes V signatures, the LSD profiles obtained with the $\chi_{\text{low}}^{\text{standard}}$ sub-mask remain featureless. One possible reason for this may be a dilution effect of the magnetic field in the upper atmosphere. Whatever the reason for it may be, the lack of Stokes V signatures in the LSD profiles obtained from lines with low excitation potential is a proof that mixing together atomic lines formed in different atmospheric layers can have a serious impact when investigating surface magnetism in pulsating stars hosting extended atmospheres wherein shockwaves propagate. The valuable result from this new approach for the analysis of the surface magnetic field is then a better definition of the Stokes V profiles which originate at the level of the photosphere.

Considering what has been said so far, the $\chi_{\text{high}}^{\text{standard}}$ sub-mask appears to be a better choice when analysing the magnetic field at the surface level. The exact same logic applies to the observations obtained near a deep minimum light, for which we constructed a $\chi_{\text{high}}^{\text{cool}}$ mask by extracting from the *cool* mask the lines with $\chi \geq 2$ eV.

4.3 The origin of circular polarization

Using, respectively, the $\chi_{\text{high}}^{\text{standard}}$ or $\chi_{\text{high}}^{\text{cool}}$ mask, we applied this refined LSD method to the Narval observations of R Sct in circular polarization in order to extract the mean polarized signatures (Stokes V profiles). The resulting LSD profiles are shown in Fig. 10 and discussed in Section 4.4. When present, the mean Stokes V signatures are typically weak, of the order of 5×10^{-5} the intensity of the unpolarized continuum. Clear Stokes V signatures are found for example in 2014 July and September, in 2015 April and August, in 2016 May, and in 2018 June. In some observations, however, there is no trace of a Stokes V signature, for example in 2016 September and in 2017 April and August.

Since we are dealing with faint polarized signatures obtained with Narval, an effect that must be taken into consideration is *cross-talk*, or the contamination of circular polarization by linear polarization and vice versa. In practice, this effect is most notable in stars that have strong net linear polarization and weak circular polarization in their spectrum (as it is the case for R Sct, see Section 5). The cross-talk on Narval has been measured from regular observations of the Ap star γ Equ. It has been estimated to be of the order of 3 per cent from 2009 observations (Silvester 2012), and stabilized below 1.5 per cent from 2016 observations (Mathias et al. 2018). Furthermore, Tessore et al. (2017) performed a dedicated observational procedure on the red supergiant μ Cep (exhibiting Stokes U & Q signatures stronger than Stokes V signals). From 2015 to 2017 observations, these authors could model the cross-talk, and they obtained, respectively, 3.6 and 1.4 per cent, for Q to V and U to V , i.e. a cross-talk level consistent with the one obtained from the Ap star γ Equ (those results also confirmed the cross talk reciprocity between linear and circular polarization signals). So in the epoch of our R Sct observations (2014–2019), we can safely consider the cross-talk level of Narval (from linear to circular, and reciprocally) was at most of the order of 3 per cent. In the following, we have considered a cross-talk level of 3 per cent.

In order to check if the Stokes V signatures observed in R Sct may be due to cross-talk from linear polarization, we compared the Stokes U , Q , and V LSD profiles obtained on 2014/09/01-02. These exact observations were used because (1) they all show strong and clear signatures in their respective Stokes parameter, and (2) they were made very close in time to each other. This comparison is shown in Fig. 11, where the Stokes V signal is amplified 10 times in order to be more easily comparable to the much stronger U & Q signals. In this figure, we also show the maximum expected level

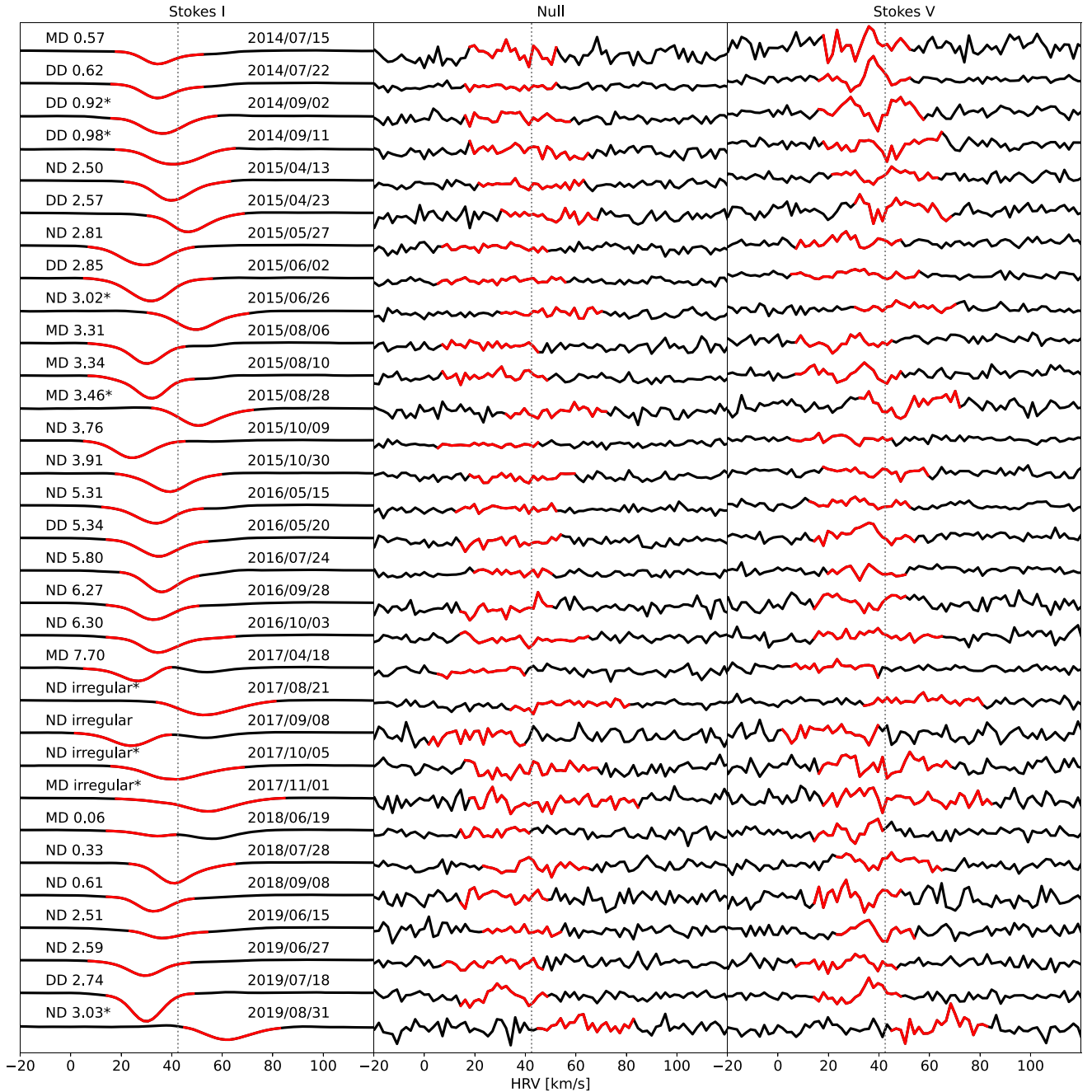


Figure 10. LSD profiles of R Sct in circular polarization using only atomic lines with $\chi \geq 2$ eV. The Stokes I , null, and Stokes V profiles of the observations are stacked vertically in the left, middle, and right column, respectively, with the date phase and detection type indicated just above their corresponding Stokes I profile. Observations treated with the *cool* mask are noted with a symbol (*). The signal (in Stokes I , null and Stokes V) within the interval of computation of the longitudinal magnetic field is colored in red. In each panel, the radial velocity of the star $v_{\text{rad}} = 42.47 \text{ km s}^{-1}$ (Kunder et al. 2017) is indicated with a dashed vertical gray line.

of cross-talk contribution from both the Stokes Q (in dashed blue) and U (in dashed red), which is below the level of the Stokes V signature observed. This shows that the observed circular polarization signal cannot be due to cross-talk, and must instead be of stellar origin.

To test if the Stokes V signal found in the LSD profiles of R Sct is due to the Zeeman effect, we performed three tests using LSD with different line masks, as it has been proposed by Mathias et al. (2018). The tests aimed to check if:

- (i) Spectral lines with high effective Landé factors (g_{eff}) show stronger Stokes V signatures than those with low g_{eff} ;
- (ii) Strong lines (ones that have a central depth larger than the average) show stronger Stokes V signatures than weak ones do;
- (iii) Spectral lines formed at longer wavelengths show stronger Stokes V signatures than those formed at shorter wavelengths.

To perform the first test, each of the two line masks ($\chi_{\text{high}}^{\text{standard}}$ and $\chi_{\text{high}}^{\text{cool}}$) was split into two sub-masks of high and low g_{eff} using the

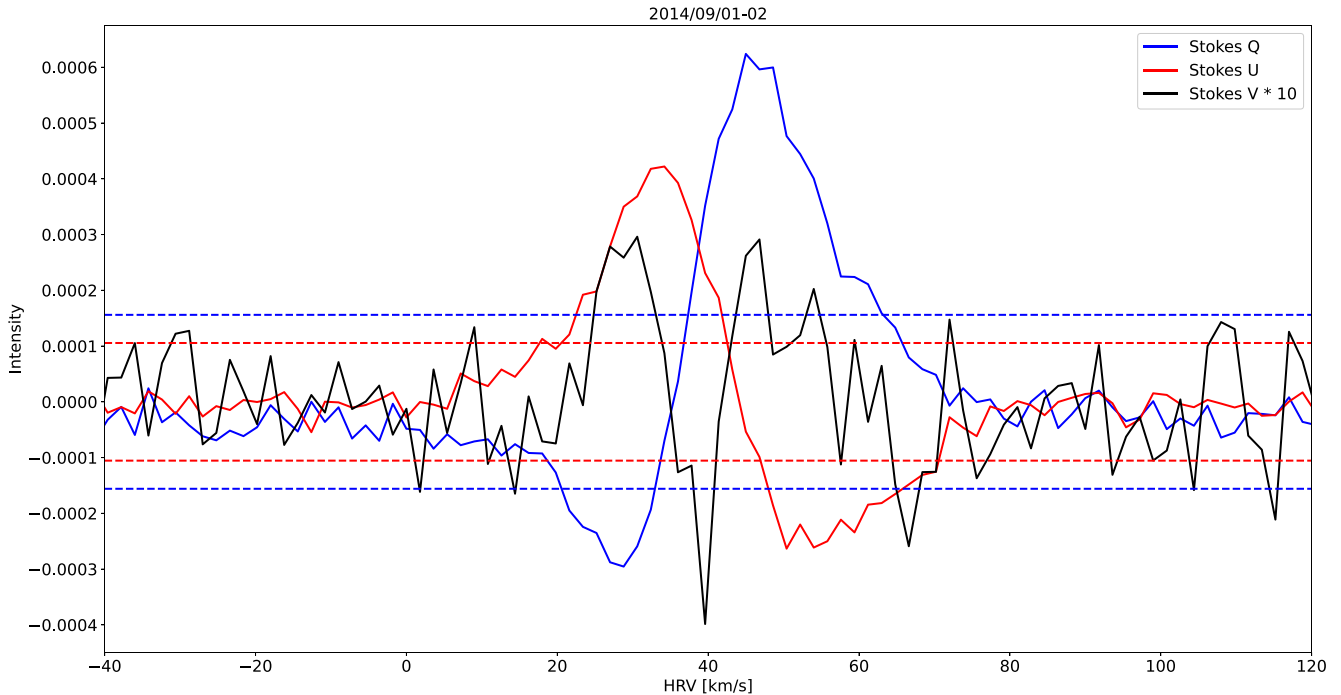


Figure 11. LSD profiles of R Sct: Stokes Q (solid blue) and U (solid red), obtained on 2014/09/01, and Stokes V (solid black, magnified 10 times) obtained on 2014/09/02. The horizontal dashed blue and red lines indicate the maximum expected level of pollution due to crosstalk by the Stokes Q and U signal, respectively, which corresponds to 3 percent of the maximum signal. This 3 percent level is also magnified 10 times in the figure in order to compensate the magnification of the Stokes V signal. It can be seen that the circularly polarized profile is above the maximum expected crosstalk level, with the three peaks at 28, 40, and 45 km s^{-1} being, respectively, 1.6, 2.1, and 1.5 times above it, ruling out the possibility that the Stokes V signal is measured due to crosstalk from linear polarization.

median value $g_{\text{eff}} = 1.2$ as the limit. For the observations where a Stokes V signature was already found using, respectively, the $\chi_{\text{high}}^{\text{standard}}$ or $\chi_{\text{high}}^{\text{cool}}$ mask, we applied the LSD process using the respective sub-masks for high and low g_{eff} and then compared the results. We found that the degree of circular polarization is indeed stronger for lines with high g_{eff} . We performed the other two tests in a similar manner, using the median values of line depth (0.66) and wavelength (446 nm) as limits. The line depth test also showed that strong lines are more strongly polarized in Stokes V than weak ones, which according to Mathias et al. (2018) favours the Zeeman origin of the circularly polarized signal. However, the wavelength test was inconclusive as it did not yield any well-defined circularly polarized signatures. Examples of the results of the tests are shown in Fig. 12.

Based on these results and considering that the circularly polarized signals are of stellar origin, we conclude that the observed Stokes V profiles are of Zeeman origin and that they indicate the presence of a surface magnetic field in R Sct.

4.4 Magnetism at the photospheric level

To constrain the analysis of the LSD profiles, and more specifically, the Stokes V signatures, to the level of the photosphere, we computed the LSD profiles for the Narval observations in circular polarization using the $\chi_{\text{high}}^{\text{standard}}$ and $\chi_{\text{high}}^{\text{cool}}$ masks, the latter being used for the observations obtained close to a deep minimum where TiO bands are present in the spectra. These masks were built as described in Section 4.2 and the resulting LSD profiles are shown in Fig. 10. Generally, the LSD profiles obtained for $\chi \geq 2$ eV resemble those obtained using the full *standard* and *cool* masks. The Stokes V profiles

obtained by using only high excitation potential lines however are more well-defined. This result is in agreement with the assumption of the zones of formation described in Section 4.2. It also shows that the magnetic field at the surface level differs from that in the higher atmosphere, otherwise the Stokes V profiles presented in Fig. 10 and the ones we obtain with the full line masks would be identical (see Fig. 9). For some particular dates (2015/08/28, 2016/05/20) it is also possible to notice a signature when using the χ_{high} masks, while it is not apparent with the full ones. In Fig. 10 it can be seen that for some observations (e.g. 2014/07/22, 2016/05/20) where the LSD intensity profile shows a double-peak structure, the Stokes V signature is clearly only associated with the blueshifted lobe. We propose that this magnetic field detection may be indeed associated with an ascending global motion of the photosphere caused by a radiative shock wave propagating outwards. As previous studies of cool pulsating stars by Lèbre et al. (2015) and Sabin et al. (2015) have suggested, the propagation of a shock wave may locally amplify a weak surface magnetic field due to a compression of the magnetic field lines.

The fact that in Fig. 10 a few observations still show a double-peak Stokes I profile (e.g. 2017/04/18 and 2017/09/08) indicates that the χ_{high} mask does not fully constrain the LSD process to the near-photospheric layers (otherwise all LSD intensity profiles would have the shape of a single Gaussian). This most likely means that the 2 eV limit may be too low, and a higher threshold is necessary in order to fully isolate the contribution of the near-photospheric layers in the computation of the LSD profiles. However, setting the excitation potential limit higher would further limit the number of lines in the mask, which would in turn decrease the SNR of the LSD profiles.

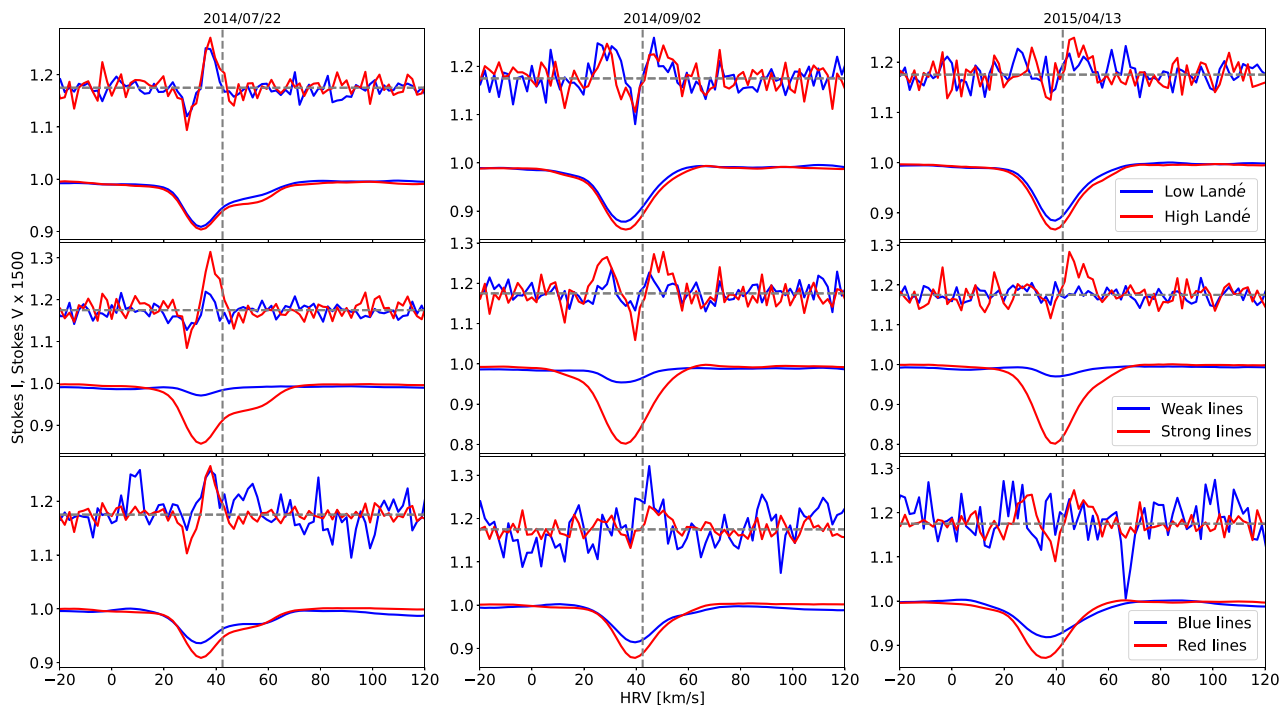


Figure 12. Comparison of a sample of LSD profiles of R Sct computed with different sub-masks to test (through the Landé factor g_{eff} , line depth, and wavelength in the left, middle, and right column, respectively) the Zeeman origin of the Stokes V signal (see Section 4.3). Each column represents Stokes V profiles computed with three different pairs of submasks for a single date of observation: 2014/07/22 is obtained just after a maximum visual brightness, 2014/09/02 corresponds to a deep minimum, and 2015/04/13 is obtained between a maximum and a shallow minimum. For each observation, the radial velocity of the star $v_{\text{rad}} = 42.47 \text{ km s}^{-1}$ (Kunder et al. 2017) is indicated with a dashed vertical grey line. The Stokes V profiles are shifted vertically and amplified 1500 times for display purposes, and their zero-level is indicated with a horizontal dashed grey line.

From Fig. 10, a rough estimation can be made of the typical time-scale of Stokes V variability. Let us consider the data from 2015 (set 2). There, a signal appears to be present in the beginning of April, which is not visible in May and June. It then reappears in August and vanishes again in October. From this variation, a rough time-scale of 2–3 months can be deduced, which is similar to the shock apparition time-scale (whatever main or secondary shock). This 2–3 month time-scale does not contradict the rest of the whole data set: for example the two observations of 2014 September show that the Stokes V signal may persist for at least one week. On the other hand, the signal obviously changes quicker than on time-scales ≥ 1 yr.

From the LSD profiles shown in Fig. 10, we computed the longitudinal component B_l using the *specpolFlow* package that uses the first-order moment method (Donati et al. 1997). For those observations that show a double-peak Stokes I profile, the velocity range of the B_l computation was limited so that only the blue peak is selected. The velocity range of B_l calculation for each observation can be seen in red in Fig. 10. The resulting B_l values, along with their error of estimation, are presented in Table 2.

The temporal evolution of the longitudinal magnetic field $B_l(t)$ is presented in Fig. 13 together with the visual light curve. It can be seen in this figure that the strength of the longitudinal magnetic field varies in time. Looking back at Fig. 10, it can also be seen that the Stokes V profiles vary in position relative to the intensity profile.

The first half of the data set, before the irregular portion of the light curve (delimited by the dashed red vertical lines in Fig. 1), contains 20 observations, of which 11 show a detection in Stokes V (6 of which are definite). The B_l varies roughly between -1.8 G (2014/09/11)

and 1.2 G (2015/04/23) in this first part of the observational data-set. For 3 dates – 2014/07/22, 2015/08/06, 2016/05/20 – the Stokes V signature appears to be associated only with the blueshifted lobe of the intensity profile. During the irregular part of the light curve, none of the 4 available observations show a clear polarized signature in Stokes V , except for a marginal detection on 2017/11/01. In the last part of the data set, after the irregular portion of the light curve, only 2 out of 7 observations show signatures in Stokes V : 2018/06/19 (MD) and 2019/07/18 (DD). Some of these results should however be considered with caution. Indeed, the standard FAP analysis may be inappropriate for weak signals such as those considered here. As recalled by Vio, Vergès & Andreani (2017), ‘it does not provide the probability that a given detection is spurious but rather the probability that a generic peak due to the noise in the filtered signal can exceed, by chance, a fixed detection threshold.’. For example, the ‘non-detection’ on 2019/08/31 may be regarded by naked-eye inspection as a tentative detection.

For those observations where the Stokes I LSD profile has a double-peak profile and a Stokes V signature is present, the latter is always associated with the blueshifted component of the Stokes I profile. This suggests that the detected magnetic field is associated with the material being lifted upwards by the passing shockwave, in support of the hypothesis that the magnetic field lines are being compressed in the shock front, which locally amplifies the surface magnetic field. However, no clear correlation exists between the longitudinal magnetic field strength and the photometric phase of the star. This suggests that the observed variability of the longitudinal magnetic field is not uniquely due to amplification caused by the propagation of shockwaves, but is also a product of a non-

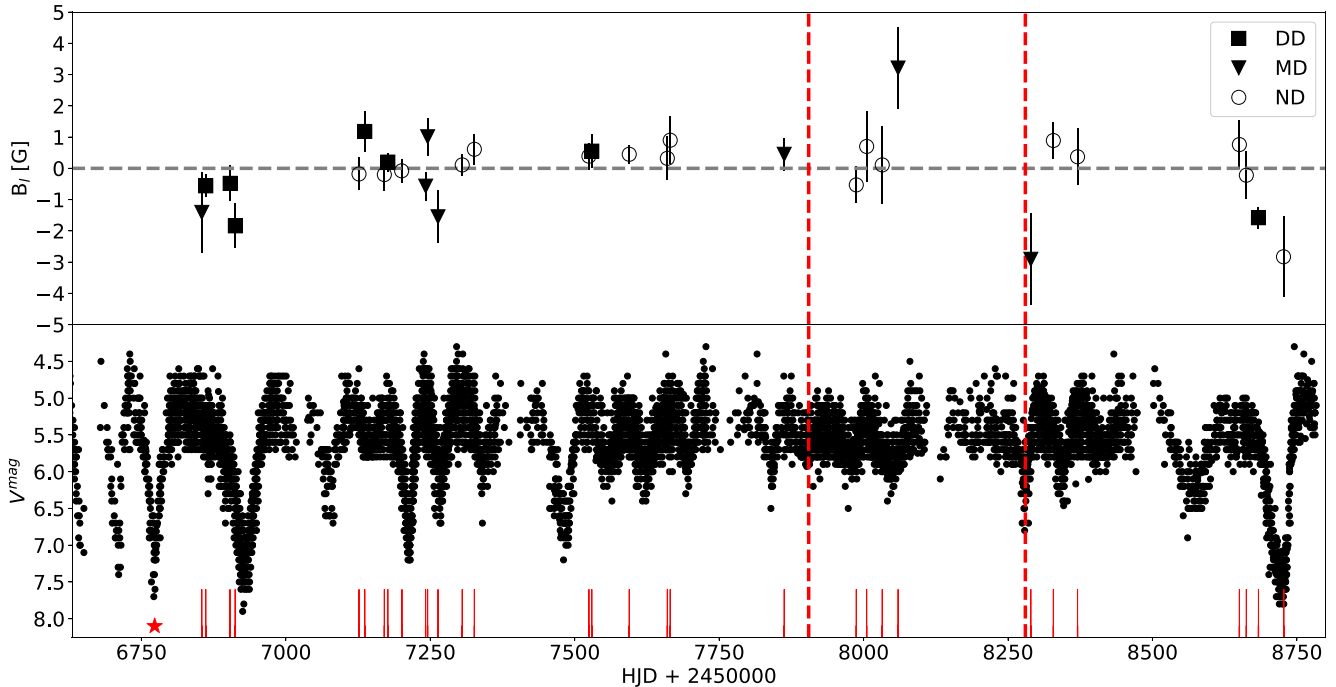


Figure 13. Temporal evolution of the longitudinal component of the magnetic field $B_l(t)$ (upper panel) and light curve (bottom panel) of R Sct. In the upper panel, the different symbols represent the different types of detections, described in Section 2.2.3: DD, MD, and ND. The red vertical lines in the bottom panel indicate the time of Narval observations that contain Stokes V measurements, and the red star indicates the date considered as the start of period 0 (see Section 2.1). The dashed vertical red lines indicate the approximate beginning and end of the irregular part of the light curve.

homogeneous and variable magnetic structure at the surface level of the star.

5 LINEAR POLARIZATION

We computed the LSD profiles of the Narval observations in linear polarization listed in Table 1 using the full *standard* and *cool* masks as described in Section 2.2 (without discriminating atomic lines by their excitation potential). We find clear linearly polarized signatures in almost all of our Narval observations, confirming the first detection of such profiles reported previously by Lèbre et al. (2015). When present, these signatures usually have amplitudes of about $1\text{--}2 \times 10^{-4}$ of the level of the unpolarized continuum (about 10 times stronger than the observed Stokes V signatures). A few examples of the obtained LSD profiles are presented in Fig. 14. In this figure, Stokes Q and U signatures that vary in both shape and amplitude can be appreciated. It can also be seen that the signatures vary in position with respect to the Stokes I profile. For example, on 2014/09/01 the signal appears more or less centered on the Stokes I profile, while on 2015/10/08 it appears redshifted, and on 2016/06/22 it is blueshifted.

Net linear polarization within atomic spectral lines has been discovered in RSG stars. For example, Aurière et al. (2016) have detected the presence of Stokes Q & U signatures in the spectrum of Betelgeuse, and have shown that the origin of these signatures is depolarization of the continuum in the spectral lines. According to these authors, this is possible due to the presence of surface brightness inhomogeneities in Betelgeuse, which they suspect to be giant convective cells.

Linearly polarized signatures have also been detected by Lèbre et al. (2014) in another cool evolved low mass star which is known to host strong pulsations, the Mira variable χ Cyg. López

Ariste et al. (2019) showed that the Stokes Q & U spectra of χ Cyg is dominated by intrinsic polarization, with only a negligible contribution from continuum depolarization. López Ariste et al. (2019) also demonstrated that the linear polarization in χ Cyg can only be explained by asymmetric velocity fields caused by the shocks, which locally enhance the Stokes Q & U signatures.

The origin of linear polarization in the spectrum of R Sct may or may not be similar to that of χ Cyg or Betelgeuse. Further insight on the nature of linear polarization in R Sct may be gained by detailed inspection of the polarized signal found in individual spectral lines, such as, for example, the sodium D-doublet (see e.g. Stenflo 1996). In this work, the linearly polarized LSD profiles are only used in order to check for cross-talk between linear and circular polarization in the available Narval observations (see Section 4.3), in order to confirm the stellar origin of the Stokes V signal. The analysis of the Stokes Q and U profiles of R Sct, and their origin, is to be done in a future study not in the scope of this paper.

6 SUMMARY

In this work, the longest monitoring of the RV Tauri variable star R Sct ever performed using high resolution spectropolarimetry is presented. Circular polarization signatures are detected in several observations and their stellar and Zeeman origin is confirmed. The time-scale of variation of these signatures appears to be of a few months, similar to the time-scale of the stellar pulsation. The differences between the dynamics of the lower (near-photospheric) and upper layers of the extended atmosphere of R Sct are presented. These differences introduce the need for a refined approach for the application of the LSD method when investigating the presence of a magnetic field at the stellar surface. Such an approach is

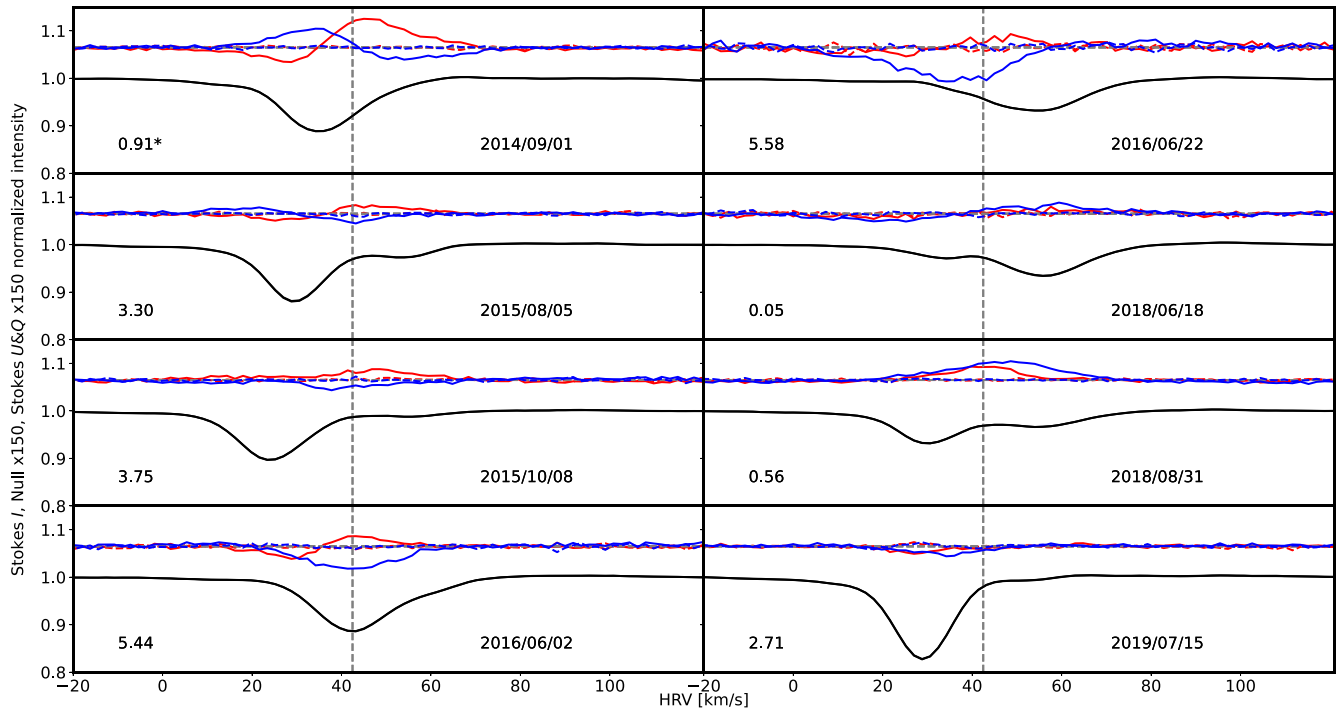


Figure 14. Some LSD profiles of R Sct in linear polarization. The phase and date of observation are indicated for each panel, as in Fig. 10. Stokes Q profiles are shown in red and Stokes U profiles – in blue, and their respective null profiles are shown in the same colours with dashed lines. Both the polarized Q & U profiles and their corresponding null profiles are shifted vertically and magnified 150 times for display purposes.

suggested and applied to the observational data set. LSD profiles constructed from lines formed mostly in the near-photospheric layers of the atmosphere are produced, and from their Stokes V signatures, the longitudinal magnetic field is measured. When the Stokes I LSD profile shows a double-peak profile, the Stokes V signature, when present, appears to be always associated with its blueshifted lobe, suggesting a connection between the shockwave propagating outwards from the photosphere and the detection of a surface magnetic field, perhaps due to compression of magnetic field lines in the shock front.

ACKNOWLEDGEMENTS

This work was supported by the ‘Programme National de Physique Stellaire’ (PNPS) of the French *Centre national de la recherche scientifique / L’institut national des sciences de l’Univers* (CNRS/INSU) co-funded by the *Commissariat à l’énergie atomique et aux énergies alternatives* (CEA) and the *Centre national d’études spatiales* (CNES). LS acknowledges support by the Marcos Moshinsky Foundation (Mexico). SG and AL thank the University of Montpellier for its support through the I-SITE MUSE (*Montpellier Université d’Excellence*) project *MAGEVOL*. We thank F. Herpin and A. Chiavassa for their valuable comments on the text. We also thank the referee, Gregg Wade, for his valuable comments and remarks which significantly helped us improve this paper. Based on observations obtained at the *Télescope Bernard Lyot* (TBL) at Observatoire du Pic du Midi, CNRS/INSU and Université de Toulouse, France. We acknowledge with thanks the variable star observations from the AAVSO International Database contributed by observers worldwide and used in this research.

DATA AVAILABILITY

The Narval observations used in this study are publicly available through the *PolarBase* online data base of spectropolarimetric observations: <http://polarbase.irap.omp.eu/>.

The AAVSO visual light curve can be obtained from the AAVSO website: <https://www.aavso.org/>.

REFERENCES

- Alvarez R., Jorissen A., Plez B., Gillet D., Fokin A., 2000, *A&A*, 362, 655
 Alvarez R., Plez B., 1998, *A&A*, 330, 1109
 Aurière M., 2003, in Arnaud J., Meunier N., eds, *EAS Publ. Ser. Vol. 9, Magnetism and Activity of the Sun and Stars*. Cambridge Univ. Press, Cambridge, p. 105
 Aurière M. et al., 2016, *A&A*, 591, A119
 Blackman E. G., 2009, in Strassmeier K.G., Kosovichev A.G., Beckmann J., eds, *Proc. IAU Symp. 259, Cosmic Magnetic Fields: from Planets to Stars and Galaxies*. Kluwer, Dordrecht, p. 35
 Decin L. et al., 2020, *Science*, 369, 1497
 Donati J.-F., Semel M., Carter B., Rees D. E., Collier Cameron A., 1997, *MNRAS*, 291, 658
 Georgiev S., Lèbre A., Josselin E., Konstantinova-Antova R., Morin J., 2020, *Astron. Nachr.*, 341, 486
 Gillet D., Burki G., Duquenois A., 1990, *A&A*, 237, 159
 Gillet D., Duquenois A., Bouchet P., 1989, *A&A*, 215, 316
 Gustafsson B., Edvardsson B., Eriksson K., Jørgensen U. G., Nordlund Å., Plez B., 2008, *A&A*, 486, 951
 Josselin E., Plez B., 2007, *A&A*, 469, 671
 Jura M., 1986, *ApJ*, 309, 732
 Kipper T., Klochkova V. G., 2013, *Balt. Astron.*, 22, 77
 Kunder A. et al., 2017, *AJ*, 153, 75

- Kupka F., Piskunov N. E., Ryabchikova T. A., Stempels H. C., Weiss W. W., 1999, *A&AS*, 138, 119
- Lèbre A., Gillet D., 1991a, *A&A*, 246, 490
- Lèbre A., Gillet D., 1991b, *A&A*, 251, 549
- Lèbre A., Aurière M., Fabas N., Gillet D., Herpin F., Konstantinova-Antova R., Petit P., 2014, *A&A*, 561, A85
- Lèbre A. et al., 2015, Proc. IAU Symp. 305, Full Stokes IQUV Spectropolarimetry of AGB and Post-AGB Stars: Probing Surface Magnetism and Atmospheric Dynamics. Kluwer, Dordrecht, p. 47
- López Ariste A. et al., 2019, *A&A*, 632, A30
- Mathias P. et al., 2018, *A&A*, 615, A116
- Plez B., 2012, Astrophysics Source Code Library, record ascl:1205.004
- Sabin L., Wade G. A., Lèbre A., 2015, *MNRAS*, 446, 1988
- Schwarzschild M., 1952, in Oosterhoff P., ed., Transactions IAU VIII. Cambridge Univ. Press, Cambridge, p. 811
- Silvester J., Wade G. A., Kochukhov O., Bagnulo S., Folsom C. P., Hanes D., 2012, *MNRAS*, 426, 1003
- Stenflo J. O., 1996, *Solar Phys.*, 164, 1
- Tessore B., Lèbre A., Morin J., Mathias P., Josselin E., Aurière M., 2017, *A&A*, 603, A129
- Vio R., Vergès C., Andreani P., 2017, *A&A*, 604, A115
- Wallerstein G., Cox A. N., 1984, *PASP*, 96, 677

This paper has been typeset from a $\text{\TeX}/\text{\LaTeX}$ file prepared by the author.